Effects of the $Be_{22}W$ phase formation on hydrogen retention and blistering in mixed Be/W systems*

Jin-Li Cao(曹金利)[1], Bing-Ling He(赫丙龄)[2], Wei Xiao(肖伟)[1,3,†], and Li-Gen Wang(王立根)[3]

[1] *School of Materials Science and Engineering, University of Science and Technology Beijing, Beijing* 100083, *China*
[2] *College of Physics and Electronic Engineering, Xinxiang University, Xinxiang* 453003, *China*
[3] *State Key Laboratory of Nonferrous Metals and Processes, General Research Institute for Nonferrous Metals, Beijing* 100088, *China*

(Received 23 January 2017; revised manuscript received 23 March 2017; published online 17 May 2017)

We have performed first-principles density functional theory calculations to investigate the retention and migration of hydrogen in $Be_{22}W$, a stable low-W intermetallic compound. The solution energy of interstitial H in $Be_{22}W$ is found to be 0.49 eV lower, while the diffusion barrier, on the other hand, is higher by 0.13 eV compared to those in pure hcp-Be. The higher solubility and lower diffusivity for H atoms make $Be_{22}W$ a potential beneficial secondary phase in hcp-Be to impede the accumulation of H atoms, and hence better resist H blistering. We also find that in $Be_{22}W$, the attraction between an interstitial H and a beryllium vacancy ranges from 0.34 eV to 1.08 eV, which indicates a weaker trapping for hydrogen than in pure Be. Our calculated results suggest that small size $Be_{22}W$ particles in hcp-Be might serve as the hydrogen trapping centers, hinder hydrogen bubble growth, and improve the resistance to irradiation void swelling, just as dispersed oxide particles in steel do.

Keywords: first-principles, hydrogen, $Be_{22}W$

PACS: 68.55.A–, 71.15.Mb, 71.15.Nc **DOI:** 10.1088/1674-1056/26/7/076801

1. Introduction

Due to its low atomic number and remarkable neutronic characteristics, beryllium (Be) has been chosen to be the primary plasma facing materials in the international thermonuclear experimental reactor (ITER).[1] As tungsten (W) is always used as the divertor armour materials, the contact of the Be and W layers is unavoidable in nuclear fusion experimental devices. In this case, subsequent re-deposition of a mixed phase Be/W can easily form during physical sputtering and chemical erosion processes, which are induced by deuterium–tritium plasma in the extreme environment of the nuclear reaction.[2] Therefore, H uptake and retention in the mixed material systems are an important issue for reliable extrapolation of in-vessel tritium retention in ITER.

Up to now, various investigations have been devoted to studying the properties of Be/W mixing by experiments,[3–6] as well as the behavior of hydrogen retention in both pure materials using theoretical simulations.[7–10] Doerner *et al.* have found that exposing W to Be-seeded deuterium (D) and D_2 plasmas can make the formation of Be–W alloys.[11,12] In addition, the Be_2W intermetallic phase can be formed at temperatures above 670 K when Be films are deposited on bulk W and annealed.[13] Conversely, by deposting W films on bulk Be, Wiltner *et al.* obtained the phase of $Be_{12}W$ within the W diffusion depth at temperatures above 1000 K.[3] Besides the experimental investigations, molecular dynamics (MD) simulations and density-functional theory calculations have also been empolyed to study the hydrogen solubility, diffusion, and interaction with vacancy in pure metals. In the work by Ganchenkova *et al.*, the authors have demonstrated that in bulk Be, hydrogen prefers the basal tetrahedral (BT) interstitial site and the migration energy is 0.40 eV. They have also found that a Be vacancy remains energetically favorable up to five hydrogen atoms.[7] In bulk W, numerous calculations have also indicated that the tetrahedral interstitial site is the favorable one for hydrogen atom and the migration energy is 0.21 eV. In contrast, a W vacancy can trap up to twelve hydrogen atoms.[8] However, the corresponding research on H behavior in Be–W materials is still lacking.[14] From a more fundamental point of view, it is interesting to analyze the influence of the secondary element (W) with rich electrons on the solubility and diffusion of H in the poor-electron element (Be). Furthermore, the physicochemical properties of the mixed materials and alloys are essential input data needed for the modeling of erosion, transport, and deposition in large-scale codes.

Undoubtedly, the studies on H behavior in the mixed materials are supposed to involve many Be/W phases. Based on the investigation of Okammoto *et al.*,[15] the Be–W phase diagram is very complex, and it includes several stable intermetallic compounds, $Be_{22}W$, $Be_{12}W$, and Be_2W. Our calculations suggest that the solution energy of W in pure Be is as

*Project supported by the National Magnetic Confinement Fusion Program of China (Grant Nos. 2014GB104003 and 2015GB105001) and the National Natural Science Foundation of China (Grant No. 51504033).

†Corresponding author. E-mail: wxiao@ustb.edu.cn

© 2017 Chinese Physical Society and IOP Publishing Ltd

high as 2.06 eV, and thus if a small amount of tungsten comes into the Be solid, $Be_{22}W$ is supposed to form instead of a solid solution or other intermetallics at the initial stage. With the increase of the tungsten concentration, other stable compounds may finally form. On the other hand, the very low concentration of W, 4.35 at.%, can make the original hcp-structure collapse, which draws our attention to the unexpected interactions between Be and W. In fact, to study H blistering in the mixed Be/W phases, it is necessary to study H behavior in all the stable intermetallic compounds and the corresponding interfaces. However, it will be a big challenge to employ first-principles calculations because of the large mismatch in the constants at the interfaces. As Allouche *et al.*[14] did for $Be_{12}W$, here we restrict our study on $Be_{22}W$, mainly including the effects of $Be_{22}W$ phase formation on hydrogen retention and blistering in the mixed Be/W phase. When high-energy hydrogen ions are implanted into the solid, it inevitably generates Frenkel pairs and cascades of atoms and vacancies, so we will consider H solubility in both interstitial sites and near vacancies. We will organize the remainder of the paper as follows. In Section 2, the theoretical methods and the computational details are described. Section 3 presents and discusses our calculated results of the behavior of the hydrogen retention and diffusion in $Be_{22}W$. Finally, a short summary is given in Section 4.

2. Methodology

The first-principles density functional theory (DFT) calculations were performed using the Vienna *ab initio* simulation package (VASP).[16–18] The electron–ion interaction was described using the projector augmented wave (PAW) method[19,20] and the exchange and correlation were treated with the generalized gradient approximation (GGA) in the Perdew–Burke–Ernzerhof (PBE) form.[21] The cut-off energy for the plane wave basis set was set to 350 eV for all of the systems. For hcp-Be metals, we employed a $4\times4\times3$ supercell consisting of 96 atoms, and a $5\times5\times5$ k-mesh in Monkhorst–Pack scheme for the integration over the Brillouin zone.[22] For cubic $Be_{22}W$, the calculated supercell contained 184 atoms and the corresponding Monkhorst–Pack mesh was $3\times3\times3$. The nudged elastic band (NEB) method was adopted to study the hydrogen diffusion behavior.[23] Five images were linearly interpolated between starting and terminal points on the migration track. In the calculations, the supercell parameters were fixed and the optimization of the atomic positions was continued until the total energy of this system was converged to less than 10^{-4} eV.

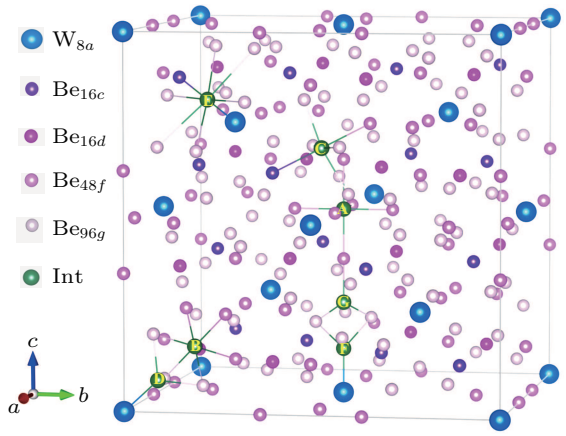


Fig. 1. (color online) The unit cell of $Be_{22}W$: W_{8a}, Be_{16c}, Be_{16d}, Be_{48f}, and Be_{96g} atoms are in blue, blueviolet, fuchsia, violet, and thistle spheres, respectively. Various interstitial (Int) sites are denoted by green spheres with letters A–G.

3. Results and discussion

3.1. Interstitial H solution and diffusion in bulk $Be_{22}W$

As shown in Fig. 1, $Be_{22}W$ has a face-centered cubic (fcc) structure (space group No. 227, $Fd\bar{3}m$) different from hcp-Be. There are 8 W and 176 Be atoms in one unit cell, in which the W atoms are located at Wyckoff positions 8a, and the Be atoms are at Wyckoff positions 16c, 16d, 48f, and 96g. To clearly display the structure of $Be_{22}W$, we highlight the W atoms with larger blue spheres, and different Be atoms are represented by blueviolet, fuchsia, violet, and thistle spheres, respectively, from higher symmetry positions to the lower ones. Compared to the unit cell of Be, we can find that with the addition of 4.35 at.% W atoms, the original hcp structure collapses, and the Be atoms are distributed into four types of lattices with different bonding environments. The lattice parameter of fcc $Be_{22}W$ is 11.56 Å, and its formation energy with reference to pure metals is −0.04 eV/atom, which testifies that the compound can be easily formed. These results are in good agreement with the previous DFT calculations.[24]

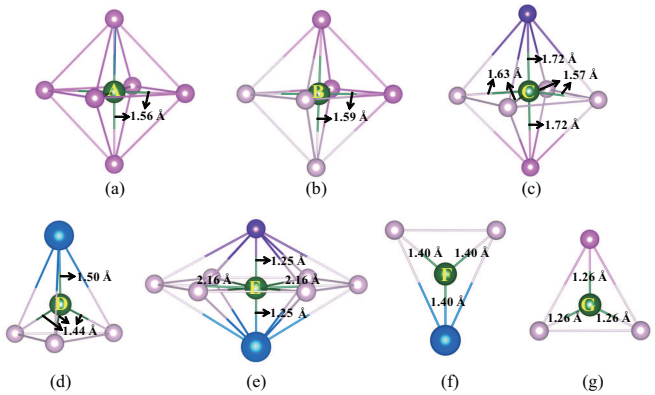


Fig. 2. (color online) (a)–(g) Zoom in to see different interstitial sites A–G in Fig. 1. Note that only the local structures, bonds, and bond lengths around the defect are displayed. For an explanation of the color spheres representing different atoms, see Fig. 1.

Table 1. The solution energies (E^{s}_{int}) and corresponding values ($E^{s}_{int,ZPE}$) considering zero point energies of interstitial hydrogen in $Be_{22}W$. The different interstitial sites are schematized by green spheres in Figs. 1 and 2.

	Interstitial sites in $Be_{22}W$							Be
Site	A	B	C	D	E	F	G	BT
E^{s}_{int}/eV	1.56	1.39	0.99	1.23	1.74	1.30	1.54	1.47
$E^{s}_{int,ZPE}$/eV	1.62	1.44	1.06	1.37	1.91	1.46	1.69	1.55

At first, we focus on the hydrogen solution at the interstitial sites of the $Be_{22}W$ matrix. Seven different interstitial sites have been considered in the calculations. These sites are denoted by green spheres with the letters A–G in Fig. 1 and also zoomed in Figs. 2(a)–2(g) for clarity. We define the solution heat of interstitial hydrogen as the energy needed to embed it into the interstitial position from the free gas state

$$E^{s}_{int}=E\left(Be_{176}W_8H\right)-E\left(Be_{176}W_8\right)-\mu\left(H\right), \quad (1)$$

where $E(Be_{176}W_8H)$ and $E(Be_{176}W_8)$ are the total free energies of systems with and without an interstitial H atom, respectively, $\mu(H)$ is the chemical potential for H, and equals to one half of the free energy of the isolated H_2 molecular, -3.38 eV, which is -3.25 eV with zero-point energy correction. At very low electron density zone, the energy cost to embedding an H atom into an electron gas is in proportion to the electron density, and H always prefers the low electron density space.[25] However, as an interstitial atom in a solid, the factor of volume and the interaction with surrounding metal atoms are also very significant. From Figs. 2(a)–2(c), we can see that the interstitial sites A and B are regular octahedral, while the site C is irregular. In addition, the site A is embraced by six chemically identical Be atoms, and the Be atoms around the sites B and C are distinct. The polyhedral volumes are 5.07 Å^3, 5.31 Å^3, and 5.83 Å^3 for the interstitial sites A, B, and C, respectively. For other interstitials, the discrepancy of the bonding environment is more obvious. The tetrahedral interstice D in Fig. 2(d) is surrounded by one W atom and three Be atoms with a volume of 1.52 Å^3. The interstitial site E in Fig. 2(e) has 2 nearest neighbors (NNs), Be and W atoms with a distance of 1.25 Å, and 6 next-nearest-neighboring (NNN) Be atoms with a distance of 2.16 Å. The interstitial sites F in Fig. 2(f) and G in Fig. 2(g) in a Be–W or Be–Be triangle with very short bond lengths are also included in our work due to the fact that the BT interstitial site possesses the lowest solution heat of 1.47 eV for hydrogen in hcp-Be.

According to formula (1), we calculate the hydrogen solution energies at the interstitial sites, and list the results in Table 1. For the interstitial site E, it has a high solution energy of 1.74 eV because of severe compression induced by the short distance between H and its NN metal atoms. The solution energies at the interstitial sites A and G are almost equal, namely, 1.54 eV and 1.56 eV. In other interstices, it ranges from 0.99 eV to 1.39 eV, lower than that in hcp-Be, which has been confirmed by the previous calculations.[26] Owing to the low atomic mass, zero-point energy (ZPE) correction of H should also be taken into account. In Table 1, we list the corresponding solution energies at different interstices corrected with ZPE and find that the trend cannot be changed. Thus we can confirm that hydrogen prefers to occupy the interstitial site C followed by D, B, and F in $Be_{22}W$, in which the lowest solution energy is 0.49 eV smaller than that in hcp-Be.

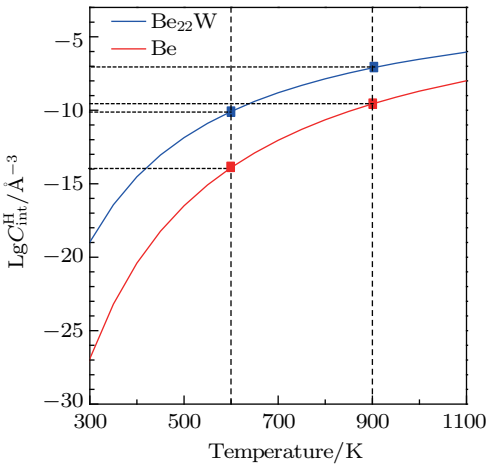


Fig. 3. (color online) Interstitial hydrogen concentration in denary logarithm as a function of temperature in different solids, $Be_{22}W$ (blue) and Be (red). The points at 600 K and 900 K in both solids are labeled by rectangles.

As we all know, the concentration of point defects such as interstitial H in the thermal equilibrium is determined by the formula

$$C^{H}_{int}(x)=A\exp\left(-\frac{E^{s}(x)}{k_BT}\right), \quad (2)$$

where A is the coordination number, E^s is the solution energy of the interstitial H,[9,26] and k_B is the Boltzmann constant. Thus, the study of the early-stage growth of H clusters can be performed by thermodynamic analysis. In Fig. 3, we directly compare the H concentrations in $Be_{22}W$ and hcp Be. Due to different lattice structures of $Be_{22}W$ and Be, here we consider their concentration in unit volume. Since there are six interstitial BT per Be unit cell with a volume of 47.52 Å^3, and 96 interstitial C in the calculated $Be_{22}W$ cell with a volume of 1544.80 Å^3, A in formula (2) is 0.13 Å^{-3} for hcp-Be, and 0.06 Å^{-3} for $Be_{22}W$. We depict the H concentration in the denary logarithm as a function of temperature in Fig. 3. It shows that the concentration of interstitial H increases with the elevated temperature, and in $Be_{22}W$ it is remarkably higher than that in pure Be, for instance, the concentration of H is 8.33×10^{-11} Å^{-3} in $Be_{22}W$, 1.26×10^{-14} Å^{-3} in Be at 600 K, and 7.66×10^{-8} Å^{-3} in $Be_{22}W$, 2.71×10^{-10} Å^{-3} in Be at 900 K, which are labeled by rectangles in Fig. 3. It means that the occupation probabilities of H in $Be_{22}W$ can reach up

to hundreds or thousands of times higher than those in a Be matrix. A high local concentration of interstitial H can appear at the formed $Be_{22}W$ compound in the Be matrix. Therefore, these inherent interstitial sites in $Be_{22}W$ can act as traps for hydrogen.

In order to detailedly elucidate the effect of tungsten addition on the H behavior in $Be_{22}W$, we should also consider the kinetics of H accumulation inside the $Be_{22}W$ solid, i.e., the diffusion and migration paths of hydrogen. Here we only consider the migration paths and barrier between the relatively stable interstitial sites using the NEB method. According to the solution energies obtained above, the initial and final positions for the diffusion paths are both interstitial sites C in $Be_{22}W$.

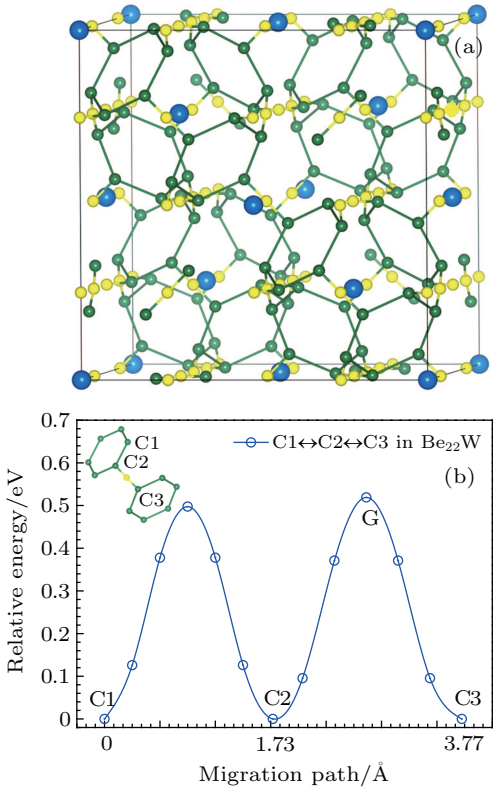


Fig. 4. (color online) Migration of interstitial hydrogen: (a) the NN interstitial sites C (green spheres) form a regular hexagon, located in the vicinity of W atoms (blue spheres). Interstitial sites G (yellow spheres) are located in the middle of the NNN interstitial site C. Note that we only represent W atoms by blue spheres for observation convenience. (b) Migration energy profiles for hydrogen migration in $Be_{22}W$ are estimated using NEB calculation. The C2 site is the NN site of interstitial site C1 with a distance of 1.73 Å, and C3 is the NNN site of site C2 with a distance of 2.04 Å.

As shown in Fig. 4(a), the interstitial sites C in the unit cell are depicted in green spheres, which form a regular hexagon plotted by green lines in the vicinity of W atoms. Each W atom has four interstice C-formed hexagons, and the center of each hexagon is Be_{16c}. Therefore, H can migrate along the regular hexagon between two NN interstitial sites C with a distance of 1.73 Å. The migration energy profiles for this path (C1↔C2) are described by blue circles on the left in Fig. 4(b). It shows that the H atom has to overcome an energy barrier of 0.50 eV when it migrates from C1 to C2 positions.

Furthermore, H needs to diffuse in full migration steps not only along the regular hexagon. By full we mean the center of mass of an H atom moves from position $\boldsymbol{P}$ (an interstitial site C2, for instance) to $\boldsymbol{P}+l\boldsymbol{a}+m\boldsymbol{b}+n\boldsymbol{c}$, where $\boldsymbol{a}$, $\boldsymbol{b}$, and $\boldsymbol{c}$ are the unit vectors with a length of lattice constant. Then, we should consider another kind of hydrogen diffusion and migration path between two NNN interstitial C sites, i.e., from C2 to C3. In Fig. 4, we show that the migration from C2 to C3 is 2.04 Å far away, and during the migration H shall pass through an interstitial site G depicted by the yellow sphere, which is just located in the center of two sites. As displayed in Fig. 4(b), the migration energy barrier along this path is 0.52 eV, which is indeed determined by the solution energy difference between C and G positions. Through the calculations of two types of diffusion and migration paths, we can obtain a migration energy barrier of 0.52 eV for H inside $Be_{22}W$.

As a comparison, we calculate the migration energy barrier of H inside the Be matrix, which is 0.39 eV from BT to nearby BT through octahedral (O) sites. The result is consistent with the previous theoretical values (0.38 eV,[7] 0.40 eV,[26] 0.41 eV[27]). This means that the migration energy barrier inside $Be_{22}W$ is 0.13 eV higher than that in the Be matrix. This lower diffusivity for H atoms in $Be_{22}W$ can impede the movement of H atoms.

Table 2. Formation energies of monovacancy in $Be_{22}W$. For comparison, the values in $Be_{12}W$, pure W, and pure Be are also listed.

Solid	Monovacancy	E^{f}_{vac}/eV
$Be_{22}W$	W_{8a}	4.91
	Be_{16c}	1.88
	Be_{16d}	1.26
	Be_{48f}	0.86
	Be_{96g}	1.03
$Be_{12}W$	W	3.00[14]
	Be	1.14–1.48[14]
Pure W	W	3.26, 3.33,[10] 3.25[14]
Pure Be	Be	1.09, 0.95,[9] 1.11[28]

3.2. H trapping of vacancy in $Be_{22}W$

When high-energy hydrogen ions are implanted into the solid, it will generate Frenkel pairs, cascades of atoms, and vacancies in the materials. Vacancies as a very low electron density zone always act as traps for hydrogen. Therefore, the studies of the vacancy formation and its interaction with H in $Be_{22}W$ are significant.

At the very beginning, we consider different types of monovacancy by removing one W atom or one of four chemically distinct Be atoms respectively in $Be_{22}W$, and their formation energies can be defined as

$$E^{f}_{vac}(W) = E(Be_{176}W_7) + \mu(W) - E(Be_{176}W_8) \quad (3)$$

or

$$E_{\rm vac}^{\rm f}({\rm Be}) = E({\rm Be}_{175}{\rm W}_8) + \mu({\rm Be}) - E({\rm Be}_{176}{\rm W}_8), \quad (4)$$

where $E({\rm Be}_{176}{\rm W}_7)$ and $E({\rm Be}_{175}{\rm W}_8)$ are the total free energies of the cell with one W and Be vacancy, and μ (W) and μ (Be) are the chemical potentials for W and Be, respectively. As $Be_{22}W$ in our work is formed at the interface between pure beryllium and tungsten solids, the chemical potential of W and Be has been taken as its value in bcc-W and hcp-Be solid.

Using formulas (3) and (4), we calculate the formation energy of monovacancy for tungsten and beryllium in $Be_{22}W$, and list these results in Table 2. In contrast with pure crystals, the formation energies of a vacancy in Be and W are also included. Since W has a much larger cohesive energy than Be, the formation of a vacancy in W can be more difficult. The calculated values are 3.26 eV and 1.09 eV, respectively, for W and Be, consistent with the previous DFT calculations[9,10,14] and the experimental values.[28] For the W monovacancy in $Be_{22}W$, it turns out that the formation energy is 4.91 eV, which shows a remarkable increase compared to the case of pure W. For the Be vacancy in $Be_{22}W$, the results are a bit more complicated. Four different types of vacancies can be formed by removing one Be_{16c}, Be_{16d}, Be_{48f}, and Be_{96g} atom respectively in the supercell. Our calculated results show that the formation energies of Be_{16c} and Be_{16d} vacancies increase to 1.88 eV and 1.26 eV, while the Be_{48f} and Be_{96g} ones decrease to 0.86 eV and 1.03 eV in comparison with the pure Be. Generally, Be_{16c} and Be_{16d} vacancies in $Be_{22}W$ can be relatively hard produced, which agrees with the work in $Be_{12}W$ by Allouche *et al.* However, the change trends of Be_{48f} and Be_{96g} vacancies are different because of the different bonding environments. In Table 2, it shows in $Be_{12}W$, three chemically distinct Be vacancies all have higher formation energies than those in pure Be, while the W vacancies have lower formation energies.[14]

To gain deeper insight into the change trend of vacancy formation in $Be_{22}W$, we now turn to the electronic structure analyses. We plot the electronic densities of states (DOS) of W atoms in $Be_{22}W$ and pure W in Fig. 5(a), and Be atoms in $Be_{22}W$ and pure Be metal in Fig. 5(b). Compared with the pure W, the broadened bands including conduction and valence bands in the DOS of tungsten in $Be_{22}W$ indicate that the W atoms suffer the compression. This is consistent with the atomic structure, in which the NN distances are 2.50 Å in $Be_{22}W$, shorter than those in pure W, 2.75 Å. Thus due to the release of the elastic energy, the tungsten vacancy should be easier to form. However, we can also see an additional peak at −0.6 eV marked by the dot ellipse in Fig. 5(a), which suggests that there are interactions between W and Be atoms in $Be_{22}W$. Furthermore, the DOS at the Fermi energy level has a decrease, see the inset in Fig. 5(a). As a consequence, the formation of tungsten vacancy in $Be_{22}W$ becomes harder. In Fig. 5(b), the p-state peaks of the valence band for Be_{16c} and Be_{16d} in the range [−4.00, −1.60] eV, which are also d-state peaks of the valence band of W in $Be_{22}W$, have a remarkable increase. Especially for Be_{16c}, the increase of peaks at −2.4 eV is simultaneous with W, and this declares the stronger interaction between them. This is mainly determined by the atomic structure, tungsten atoms being the NN of Be_{16c} with a short distance of 2.50 Å. For Be_{48f} and Be_{96g}, the top of the valence band has a weak increase, and resembles pure Be, thus the formation energy of vacancies is close to the pure metal. In addition, the DOSs at the Fermi energy level of Be_{16c} and Be_{16d} are lower than those of Be_{48f} and Be_{96g}, which suggests that Be_{16c} and Be_{16d} are harder to form.

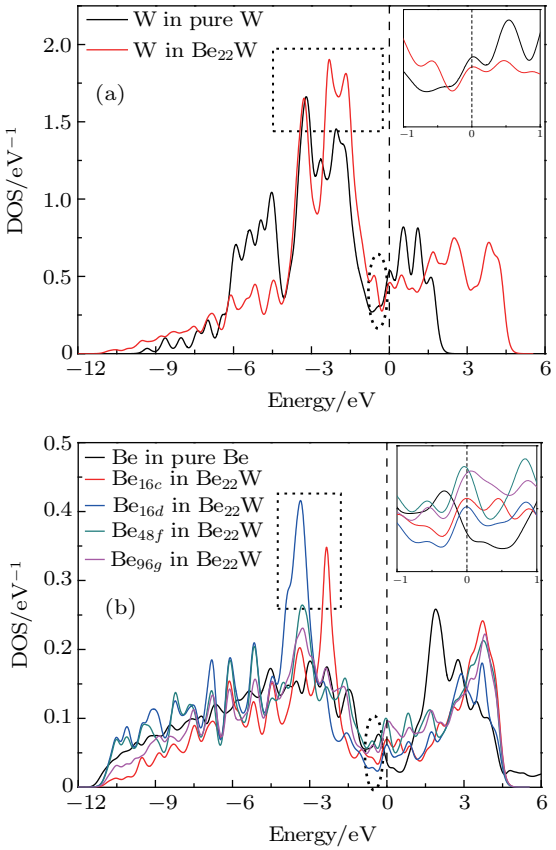


Fig. 5. (color online) Comparison of electronic density of states of (a) W atoms in $Be_{22}W$ and pure W, (b) Be atoms in $Be_{22}W$ and pure Be. The Fermi energy is set to zero denoted by black dash lines, and the DOS nearby the Fermi energy level ranging from −1 eV to 1 eV are drawn in the inset.

Table 3. Calculated distances between hydrogen and vacancy ($d_{\rm H-vac}$) and trapping energies ($E_{\rm trap}$) of various beryllium vacancies in $Be_{22}W$.

Site	hcp-Be	Be_{16c}	Be_{16d}	Be_{48f}	Be_{96g}
$d_{\rm H-vac}$/Å	1.05	1.71	0.98	1.17	0.92
$E_{\rm trap}$/eV	1.14 (1.08[9])	0.34	0.39	0.63	1.08

Hydrogen can facilitate the preservation of superabundant vacancies in a large variety of metals and alloys,[29] and vice versa, vacancies have been found to trap hydrogen.[8,9] Therefore, it is necessary to investigate the interaction between H

and the vacancy. We define the trapping energy ($E_{\rm trap}$) to characterize the energy required for moving an H atom into the vicinity of a beryllium vacancy from a remote interstitial site C

$$E_{\rm trap}({\rm Be}) = E({\rm Be_{176}W_8H}) + E({\rm Be_{175}W_8}) - E({\rm Be_{175}W_8H}) - E({\rm Be_{176}W_8}), \quad (5)$$

where $E({\rm Be_{175}W_8H})$ is the total free energy of systems when H is near one Be atom vacancy. Here, we just consider a beryllium monovacancy due to the large formation energy of the tungsten vacancy. In the alloy calculations, the H atom is placed at and off the center of the monovacancy, and the optimized atomic configurations suggest that H atoms prefer to stay at 1.71 Å, 0.98 Å, 1.17 Å, and 0.92 Å away from the center of $\rm Be_{16c}$, $\rm Be_{16d}$, $\rm Be_{48f}$, and $\rm Be_{96g}$ vacancy, respectively. We list the distances between H and the vacancy and the calculated trapping energies of various beryllium vacancies in Table 3. The trapping energy of $\rm Be_{96g}$ vacancy is 1.08 eV, slightly lower than that of pure beryllium, 1.14 eV. Nevertheless, for three other types of beryllium vacancies, the trapping energies of beryllium vacancy, $\rm Be_{16c}$, $\rm Be_{16d}$, and $\rm Be_{48f}$ for H atoms are 0.34 eV, 0.39 eV, and 0.63 eV, respectively, markedly lower than that of pure beryllium. Among them, the low trapping energies of $\rm Be_{16C}$ and $\rm Be_{16d}$ monovacancy can be attributed to their large vacancy formation energies. The weaker trapping of a vacancy for H in $\rm Be_{22}W$ provides a less driving force to form H clusters than that in pure Be solids.

4. Conclusion

Using first-principles density calculations, we have systematically investigated the distribution and migration of H inside $\rm Be_{22}W$ solid. The solution energy of interstitial H atoms in $\rm Be_{22}W$ is 1.06 eV, which is 0.49 eV smaller than that in hcp-Be. The migration barrier of interstitial H is 0.52 eV from the most stable interstitial site C to its NNN site, larger than that in Be solid. Therefore, compared to H in pure Be solid, the larger solubility and slower diffusion of H atoms in $\rm Be_{22}W$ solid make it a potential beneficial secondary phase in hcp-Be to impede hydrogen diffusion. On the other hand, the interaction of beryllium and tungsten in $\rm Be_{22}W$ increases the formation energy of W, $\rm Be_{16c}$ and $\rm Be_{16d}$ vacancies and decreases it for $\rm Be_{48f}$ and $\rm Be_{96g}$ in comparison with the pure Be. Furthermore, we have obtained the hydrogen trapping energies of distinct beryllium vacancies in $\rm Be_{22}W$, including $\rm Be_{16c}$, $\rm Be_{16d}$, $\rm Be_{48f}$, and $\rm Be_{96g}$, which are 0.34 eV, 0.39 eV, 0.63 eV, and 1.08 eV. All are lower than that in pure Be, 1.14 eV, which provides a less driving force for the accumulation and clustering of H atoms than that in pure Be solids.

Our calculations suggest that interstitial H atoms have a lower solution energy, a higher migration energy, and are harder to accumulate into the vacancy in $\rm Be_{22}W$ than the matrix. Based on our calculations, H prefers $\rm Be_{22}W$ over pure Be solid, which can slow the growth of H clusters and bubbles in Be solid. Thus, H bubbles are dispersed and the concentrated stress may be released below the limited strength of the materials. Consequently, H embrittlement or hydrogen-related irradiation swelling could be suppressed. We can hope that the presence of $\rm Be_{22}W$ is potentially very effective to serve as a dispersed trapping center to retard the growth of H bubbles, just as the suppressing effect of oxide particles on the growth of He and H bubble in ODS steels,[30,31] and enhancing the resistance to irradiation void swelling and H embrittlement.

References

[1] Merola M 2010 *Fusion Eng. Des.* **85** 2312
[2] Perkins F W 1999 *Nucl. Fusion* **39** 2137
[3] Wiltner A, Kost F, Lindig S and Linsmeier Ch 2007 *Phys. Scr.* **T128** 133
[4] Linsmeier Ch 2007 *J. Nucl. Mater.* **363–365** 1129
[5] Baldwin M J 2007 *J. Nucl. Mater.* **363–365** 1179
[6] Lasa A, Heinola K and Nordlund K 2014 *Nucl. Fusion* **54** 083001
[7] Ganchenkova M G, Borodin V A and Nieminen R M 2009 *Phys. Rev. B* **79** 134101
[8] Ohsawa K, Goto J, Yamakami M and Yagi M 2010 *Phys. Rev. B* **82** 184117
[9] Zhang P B, Zhao J J and Wen B 2012 *J. Phy.: Condens. Matter.* **24** 095004
[10] Xiao W, Luo G N and Geng W T 2012 *J. Nucl. Mater.* **421** 176
[11] Doerner R P, Baldwin M J and Causey R A 2005 *J. Nucl. Mater.* **342** 63
[12] Doerner R P 2007 *Phys. Scr.* **T128** 115
[13] Wiltner A and Linsmeier C 2005 *J. Nucl. Mater.* **337** 951
[14] Allouche A, Fernandez N and Ferro Y 2014 *J. Phys.: Conden. Matter.* **26** 315012
[15] Okammoto H and Tanner L E 1991 *Phase Diagrams of Binary Tungsten Alloys* (Calcutta: Indian Institute of Metals)
[16] Kresse G and Furthmüller J 1996 *Phys. Rev. B* **54** 11169
[17] Kresse G and Hafner J 1993 *Phys. Rev. B* **47** 558
[18] Kresse G and Furthmüller J 1996 *Comp. Mater. Sci.* **6** 15
[19] Kresse G and Joubert D 1999 *Phys. Rev. B* **59** 1758
[20] Blöchl P E 1994 *Phys. Rev. B* **50** 17953
[21] Perdew J P, Burke K and Ernzerhof M 1996 *Phys. Rev. Lett.* **77** 3865
[22] Monkhorst H J and Pack J D 1976 *Phys. Rev. B* **13** 5188
[23] Henkelman G, Uberuaga B P and Jónsson H 2000 *J.Chem. Phys.* **113** 9901
[24] Jain A 2013 *APL Mater.* **1** 011002
[25] Puska M J, Nieminen R M and Manninen M 1981 *Phys. Rev. B* **24** 3037
[26] Zhang P B, Zhao J J and Wen B 2012 *J. Nucl. Mater.* **423** 164
[27] Allouche A, Oberkofler M, Reinelt M and Linsmeier Ch. 2010 *J. Phys. Chem. C* **114** 3588
[28] Baskes M I and Johnson R A 1994 *Model. Simul. Mater. Sci.* **2** 147
[29] Fukai Y 2003 *Phys. Scr.* **T103** 11
[30] Hsiung L L 2010 *Phys. Rev. B* **82** 184103
[31] Esteban G A 2007 *Fusion Eng. Des.* **82** 2634